Hindawi
Mathematical Problems in Engineering
Volume 2018, Article ID 7531260, 14 pages
https://doi.org/10.1155/2018/7531260

Research Article

Frequency Domain Design of a Series Structure of Robust Controllers for Multi-Input Single-Output Systems

Montserrat Gil-Martínez,[1] **Javier Rico-Azagra**,[1] **and Jorge Elso**[2]

[1]*Electrical Engineering Department, University of La Rioja, San José de Calasanz 31, 26004 Logroño, Spain*
[2]*Department of Engineering, Universidad Pública de Navarra, 31006 Pamplona, Spain*

Correspondence should be addressed to Montserrat Gil-Martínez; montse.gil@unirioja.es

Received 7 June 2018; Accepted 18 October 2018; Published 30 October 2018

Academic Editor: Jose Vicente Salcedo

The regulation of a disturbed output can be improved when several manipulated inputs are available. A popular choice in these cases is the series control scheme, characterized by (1) a sequential intervention of loops and (2) faster loops being reset by slower loops, to keep their control action around convenient values. This paper tackles the problem from the frequency-domain perspective. First, the working frequencies for each loop are determined and closed-loop specifications are defined. Then, Quantitative Feedback Theory (QFT) bounds are computed for each loop, and a sequential loop-shaping of controllers takes place. The obtained controllers are placed in a new series architecture, which unlike the classical series architecture only requires one controller with integral action. The benefits of the method are greater as the number of control inputs grow. A continuous stirred tank reactor (CSTR) is presented as an application example.

1. Introduction

In process control, it is common to find several manipulated variables regulating a single measurable output (MISO: *Multiple Input Single Output* control). Remarkable examples are distillation columns [1], chemical and biochemical reactors [2–4], heat-exchangers [5], paper-machines [6], and medical control systems [7, 8]. Recent fields of application are the automotive industry [9, 10], consumer-electronics [11, 12], and robotics and unmanned aerial vehicles [13, 14].

The architectures for MISO control can be grouped in two: the parallel [15, 16] and the series disposition of controllers. The latter (see Figure 1) originally appeared in the *habituating control* by Henson et al. [15] and the *midranging* control by Allison and Isaksson [17]. It can be seen as a generalization of the *valve position control (VPC)* for the process industry presented by Shinskey [1] and Luyben [18]. Skogestad and Postlethwaite [19] labelled it as *cascade control*. The architecture seeks a sequential loop intervention from the fastest (bottom) to the slowest (top) loop, in order to recover the set-point r at the d-disturbed output y. Besides, the fastest control variable u_2 returns to the setpoint r_{u_2} when the slowest loop resets the fastest loop (*input resetting control*). Plant models p_1 and p_2 characterise the dynamic behaviour of the output y in response to the manipulated inputs u_1 and u_2, respectively. Similarly, p_d models the response of y to the disturbance input d. The signal v has been added to account for sensor noise.

In steady state, several combinations of the manipulated inputs (u_1, u_2) could achieve the desired output $r = y$. Hence, r_{u_2} can be chosen according to different criteria, which are usually linked to efficiency, cost savings, and physical limitations. For example, midranging [17, 20] chooses r_{u_2} as the midpoint of the u_2 actuator to preserve the largest maneuvering range in the fast loop. Conversely, in the temperature (y) control of a chemical stirred tank reactor (CSTR), Luyben [21] manipulates the coolant flow to a tank jacket (u_2) around the maximum removal capacity (r_{u_2}) in such a way that the feed-flow rate (u_1) is indirectly maximized, and so is the production rate. Other works [6, 15] prefer reducing r_{u_2} as much as possible since u_2 represents a more expensive physical variable than u_1, and global plant operating expenses are dominated by steady state control actions. Parallel structures of controllers can equally attain

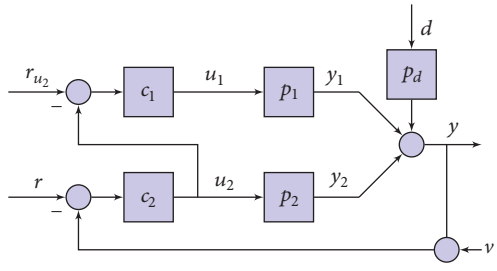

Figure 1: Classical series architecture (*midranging*).

those aims. For instance, Nájera et al. [4] shows several ways to conduct the air flow set-point (r_{u_2}) in the sludge temperature (y) control of a biochemical reactor operated by the air-flow (u_2) and the inlet sludge flow (u_1). A smaller r_{u_2} reduces direct expenses by cutting the amount of u_2. On the other hand, a higher r_{u_2} deliberately pursues a major spending of u_2 in order to force a higher u_1, which raises the production rate and makes the plant operation more profitable.

Most applications and methods in the literature show integral action in both controllers c_1 and c_2 to obtain zero steady-state tracking error in $r - y$ and $r_{u_2} - u_2$. However, the two integrators in series can make the slowest loop $c_2c_1p_1$ conditionally stable [22]. Moreover, the more manipulated inputs there are, the harder the control design becomes. This is one of the concerns of the present work. A second one has to do with the frequency bands at which each input contributes to the regulation. The location of each input inside the control structure determines which plant works in high (p_2) and low (p_1) frequencies, respectively, whereas the controllers determine the border between these two ranges. These decisions may not be trivial. As stated before, some considerations are linked to the steady-state and permitted range of the manipulated variables themselves. Others have to do with the best achievable performance according to the plant frequency responses. Most contributions in the literature solve practical examples with *ad-hoc* decisions and tailor-made design methods, although some general design methods are described in [1, 15, 22–25]. Their common approach is firstly designing the fastest loop (i.e. c_2) to achieve certain performance in the regulation of y, and then, designing the slowest loop (i.e. c_1) that takes u_2 to the setpoint r_{u_2}. One important remaining challenge is how to perform the switching-off of the fast loop since global performance or even stability may be compromised [22]. Moreover, no method has been reported on how to distribute the performance amongst more than two branches as far as the authors are aware.

Under these premises, the present work proposes a new series structure of n controllers allowing to exploit the benefits of using n manipulated inputs while avoiding the inconveniences of having integral action in all controllers. In this work, integrators appear only in the controller that is next to the plant that works at the lowest frequencies (c_1 if $n = 2$). It will be shown that this is sufficient to achieve the set-points at the output and at the $n-1$ midrange inputs with zero steady-steady error. The present work adopts a frequency domain perspective, showing how to allocate the control load among the different loops. In particular, a robust methodology is proposed in the framework of Quantitative Feedback Theory (QFT) [26–28], which includes plant uncertainty in the controller design process. The new method details how to compute the QFT bounds and how to perform a sequential loop-shaping of controllers.

The paper is organised as follows. Section 2 justifies the new series structure for MISO control. Section 3 describes the multi-input participation from a frequency domain perspective and proposes a frequency domain method to achieve robust stability and performance in the regulation of the disturbed output and midrange inputs. Section 4 illustrates the usefulness of the proposed methodology to improve the controllability of a continuous stirred tank reactor (CSTR). Finally, Section 5 presents the main conclusions.

2. A New Series Architecture

The two controlled variables in Figure 1 can be expressed in terms of the external inputs as follows (either s-Laplace or ω-frequency domains are possible for variables and functions):

$$y = \frac{l_t}{1+l_t}(r-v) + \frac{p_d}{1+l_t}d + \frac{c_1p_1}{1+l_t}r_{u_2}, \tag{1}$$

$$u_2 = \frac{c_2}{1+l_t}(r-v) + \frac{-p_d}{1+l_t}d + \frac{-c_2c_1p_1}{1+l_t}r_{u_2}, \tag{2}$$

where

$$l_t = l_2 + l_1 = c_2p_2 + c_2c_1p_1. \tag{3}$$

Let us consider: the sensor noise $v(t)$ exclusively contains high frequency components, i.e. $v(t=\infty) = v_{ss} = 0$, the p_1 and p_2 plants model self-regulating processes (absence of integrating dynamics), the r and r_{u_2} set-points take constant values, and the d disturbance is step-type. A suitable feedback design demands both $|l_t(j0)| \gg 1$ and $|l_t(j0)| \gg |p_d(j0)|$ at steady-state $s = j\omega = j0$. Besides, distinguishing the fast and slow loops requires that $|c_2(j0)c_1(j0)p_1(j0)| \gg |c_2(j0)p_2(j0)|$, i.e. $|l_1(j0)| \gg |l_2(j0)|$. Thereby, considering $(r-v)$ and d inputs in (1), a zero steady-state error at the output, $y_{ss} = y(t=\infty) = r_{ss}$ needs of $|l_t(j0)| = \infty$, which must be necessarily provided by $|c_1(j0)| = \infty$ since $|l_1(j0)| \gg |l_2(j0)|$. An integrator in c_1 does the job. Furthermore, $|c_2(j0)| = \infty$ (an integrator in c_2) is also needed to neglect the influence of r_{u_2} at y_{ss} in (1), which also preserves $|l_1(j0)| \gg |l_2(j0)|$. Regarding (2) both controllers also need integral part to achieve $u_{2_{ss}} = r_{u_{2_{ss}}}$. Beyond their usefulness for steady-state purposes, integrators become a problem for linear stability, in addition to other practical issues such as wind-up phenomena. Regarding the stability, the loop l_1 is the most troublesome since it contains two integrators, which means a phase lag of -180° at $\omega = 0$. Because of that, [22] discusses some examples of conditional stability. Achieving stable loops would become more and more challenging if more manipulated inputs were used. Let us suppose the Figure 1 structure were generalised for $n > 2$ manipulated inputs. As each c_i controller ($i = 1, \ldots, n$) should contribute with one

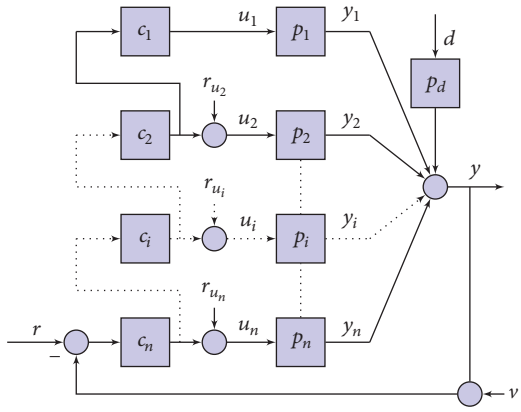

Figure 2: Series architecture for n actuators.

integrator, the most critical loop $l_1 = p_1 \prod_{i=1}^{n} c_i$ would have a phase lag of $-90^{\circ}n$ at $\omega = 0$. Thus, the loops $i > 2$ would be conditionally stable and demand lead-lag networks that would increase the order of controllers and make harder the design procedure. The new series arrangement of controllers in Figure 2 overcomes the above problems.

In the new architecture, the system output is

$$y = \frac{1}{1 + l_t}\left(l_t\,(r - v) + p_d d + \sum_{i=1}^{n} p_i r_{u_i}\right), \tag{4}$$

where

$$l_t = \sum_{i=1}^{n} l_i \tag{5}$$

is the total open-loop transfer function, which is made up of individual loops

$$l_i = p_i c_i^{*} = p_i \prod_{j=i}^{n} c_j. \tag{6}$$

This branch open-loop function l_i defines the direct path from the output set-point r to each p_i-plant contribution to the output:

$$y_i = \frac{l_i}{1 + l_t}\,(r - v - p_d d) - \sum_{j \neq i} \frac{p_j l_i}{1 + l_t} r_{u_j} + \frac{(1 + l_t - l_i)\,p_i}{1 + l_t} r_{u_i}. \tag{7}$$

Eventually, each plant is driven by

$$u_i = \frac{l_i / p_i}{1 + l_t}\,(r - v - p_d d) - \sum_{j \neq i} \frac{p_j l_i / p_i}{1 + l_t} r_{u_j} + \frac{1 + l_t - l_i}{1 + l_t} r_{u_i}. \tag{8}$$

And particularly, the manipulated input $u_{i>1}$ steady-states can be conveniently trimmed by the set-points $r_{u_{i>1}}$, while the dependent variable u_1 steady-state can be freely adapted by the control law to fight persistent disturbances d or any other kind of system unknowns. So there is not a set-point for u_1, as in classical structures. A first advantage of the new architecture is that negative comparisons of Figure 1 are no longer needed at midrange variable sum-points since the negative feedback at r sum-point suffices. This avoids unnecessary inverse gains on the controllers. A second and major advantage is that an integral action in c_1 makes $|l_t(j0)| = \infty$, which suffices to achieve $y(t = \infty) = r(t = \infty)$ (4), and to achieve $u_{i>1}(t = \infty) = r_{u_{i>1}}(t = \infty)$ (8), under the assumption of constant set-points and step-type disturbances. Furthermore, integrators are no longer needed to yield $|l_i(j0)| \gg |l_{i+1}(j0)|$. In general, c_1 must provide the number of integrators that were needed depending on the external inputs, the plants, and the prescribed steady-state tracking errors.

Inputs u_i must be conveniently arranged in the structure considering that l_n will be the fastest loop and l_1 will be the slowest loop. Feedback controllers c_i will determine the specific working frequencies for each loop l_i in the global regulation task. These frequencies also condition the time at which an upper loop disconnect a lower loop inside the structure. The next section details a frequency domain design procedure for those controllers.

There is an equivalent of the series structure (Figure 2) to a parallel one where $r - (y + v)$ would be lead to independent branches l_i (6) whose controllers would be c_i^{*}. Let us note as controllers c_i are of lower order than controllers $c_i^{*} = \prod_{j=i}^{n} c_j$, since each individual controller c_i does not need to add dynamics of high order that have been added by $c_{j>i}$. The counterpart of simpler controllers is a lower flexibility of the structure. Thus, the series structure sets the time sequence of plant intervention, while the controllers could freely allocate it in a parallel structure [16]; furthermore, this can make several plants work in the same frequency band.

3. A Robust Frequency Domain Control Design

3.1. Multi-Input Participation in the Frequency Domain. For simplicity, let us assume $p_d = 1$ and dual input $i = 2$ in the series architecture of Figure 2. A sensitivity function $S(s)$ models the desired performance for disturbance rejection $y(s)/d(s)$; Figure 3(a) depicts its magnitude frequency response $|S(j\omega)|$. The closed-loop specification $S = 1/(1 + l_t)$ can be straight away expressed in terms of the open-loop function l_t, whose magnitude frequency response $|l_t(j\omega)|$ is also depicted on Figure 3(a); ω_{gc} represents the gain crossover frequency, which quantifies the control system bandwidth. Let us remark that the maximum magnitude peak of $|S(j\omega)|$ also defines a minimum degree of stability since it bounds a distance from $l_t(j\omega)$ to the critical point (stability margins) [29]. Thereby, $|l_t(j\omega)|$ in Figure 3(a) represents the robust performance and stability to be achieved by the MISO control.

However, there are infinite pairs (l_1, l_2) that build l_t and satisfy that l_1 prevails over low frequencies and l_2 over high frequencies. An arbitrary pair is depicted on Figure 3(a),

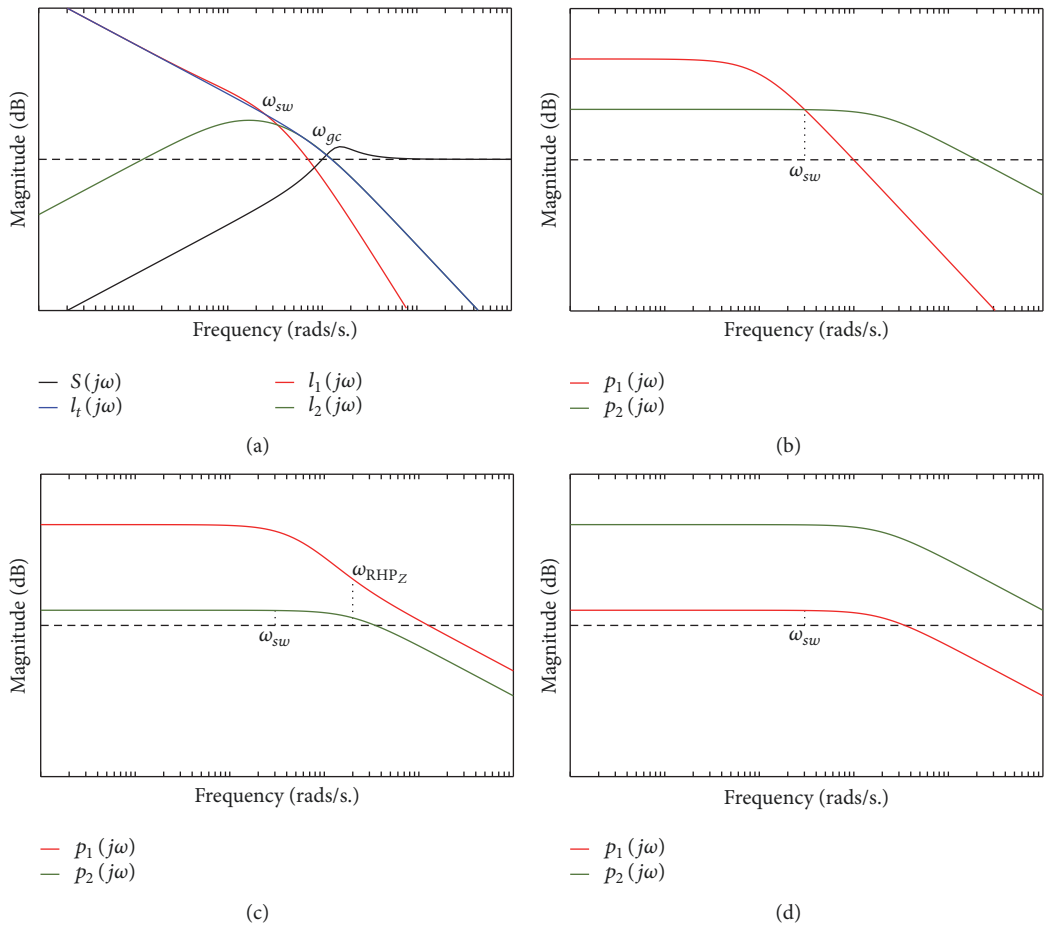

Figure 3: Frequency goals.

revealing that the switching frequency ω_{sw} must be specified by the designer. This frequency is closely related to when the fastest loop is disconnected by the slowest loop, i.e. to the time $t_{sw} \approx 4/\omega_{sw}$ that takes u_2 to recover its midrange setpoint r_{u_2}.

Saving feedback (less gain) at each branch implies each loop dominates over its frequency band. Thus, $|l_1(j\omega)|$ rolls off to $-\infty$ from $\omega \geq \omega_{sw}$ and $|l_2(j\omega)|$ rolls off to $-\infty$ before $\omega \leq \omega_{sw}$. An abruptly roll-off would require quite complex controllers (great number of poles and zeros), not only to achieve a sharp gain increment/decrement but also to guarantee system stability (let us remind that according to Bode integrals the magnitude slope is closely related to its phase lag [27]). Besides, the fact that l_t achieves sufficient stability, by means of a large enough distance of l_t to the critical point (stability margins), does not necessary imply that both l_1 and l_2 show large enough distances to the critical point. Thus, as long as stability margins are chosen in consonance with the uncertainty about plant models, it will be of interest to define sufficient stability margins for both loops, which hampers their disconnection slopes.

Other relevant points are the frequency allocation of plants in the frequency band and the best choice of ω_{sw}, which are intimately linked to the application and designer expertise. Let us describe some general examples in Figures 3(b), 3(c), and 3(d). They depict the magnitude frequency responses of plants p_1 and p_2 that have already been chosen to contribute over low and high frequency bands, respectively. It is important to remark that plants must be conveniently scaled [19] for a fair comparison. Figure 3(b) depicts two minimum phase plants with different frequency characteristics. Thus, choosing ω_{sw} at the cross-frequency where $|p_1(j\omega_{sw})| = |p_2(j\omega_{sw})|$ will make the most of both plants to achieve the required performance while saving feedback (smaller controller gains). This case is thoroughly exploited inside a parallel structure in [16]. Similarly the case depicted in Figure 3(c) also makes the most of input-output characteristics. In this case, the low-frequency gain superiority and the presence of a RHP zero in one of the plants make it the option to work at low frequencies; ω_{sw} is chosen sufficiently less than ω_{RHP_z} for an appropriated degree of stability. On the other hand, Figure 3(d) shows an apparent contradiction considering only the plant frequency responses. At a first glance p_2 should be the only plant to be involved in the regulation task inside a SISO control structure, since p_1 will not improve the performance. In fact, p_1 will demand a higher control action than p_2 would have at the steady-state. In this case, the trick s u_1 physically represents a much less expensive actuation than u_2, which justifies its intervention.

In summary, quantitative and frequency design methods can be of great help to guide the control designer. Particularly,

the loop-shaping of $l_1(j\omega)$ and $l_2(j\omega)$ appears to be the wiser approach.

3.2. Robust Control Problem Statement. Plant model uncertainty and unknown disturbances justifies feedback [26, 30]. The explicit consideration of uncertainty in the design makes the control robust. Let us consider m uncertain parameters in the set of $n+1$ plant models $p_{i=1,\dots,n}$, p_d of Figure 2. And take $\mathbf{q}_j$ as a vector in the set of all their possible values $\mathcal{Q} \in \mathbb{R}^m$. Thus, the MISO uncertain system is defined

$$\mathcal{P} = \left\{\mathbf{P}\left(s, \mathbf{q}_j\right) : \mathbf{q}_j \in \mathcal{Q}\right\}, \tag{9}$$

where $\mathbf{P}$ is a $1 \times (n+1)$ vector in the uncertain set.

Hence, a set of time responses (4) is possible when a d-disturbance happens. A performance model $W_d(s)$ is chosen to limit those responses. According to QFT principles, the robust performance for disturbance rejection can be expressed in the frequency domain $s = j\omega$, $\omega = [0, \infty)$ as

$$\left|T_d\right| = \left|\frac{y}{d}\right| = \left|\frac{p_d}{1 + l_t}\right| \le \left|W_d\right|; \quad \forall \mathbf{P}. \tag{10}$$

And the robust stability in $s = j\omega$, $\omega = [0, \infty)$ is being expressed in this work by the set

$$\left|T_{s_i}\right| = \left|\frac{l_i / \left(1 + \sum_{j \ne i} l_j\right)}{1 + l_i / \left(1 + \sum_{j \ne i} l_j\right)}\right| = \left|\frac{l_i}{1 + l_t}\right| \le W_{s_i}, \quad i = 1, \dots, n; \ \forall \mathbf{P}. \tag{11}$$

For a particular ω frequency, each inequality of (11) defines a forbidden region around the critical point -1 that cannot be violated by $l_i = c_i^* p_i / (1 + \sum_{j \ne i} l_j)$. In this way the prescribed degree of stability can be linked to the uncertainty of each plant p_i. Particularly, to achieve certain gain margin GM_i above p_i gain uncertainty, the upper tolerance is chosen as

$$W_{s_i} = \frac{1}{\mathrm{GM}_i - 1}, \quad \mathrm{GM}_i > 1. \tag{12}$$

To enforce a phase margin PM_i above p_i phase uncertainty, the upper tolerance becomes

$$W_{s_i} = \frac{1}{2 \sin\left(\mathrm{PM}_i / 2\right)}. \tag{13}$$

Then robust stability (11) is straight forward related to individual loops, while robust performance (10) is a collaborative task among loops. Thus, the robust performance must be distributed among the loops along the frequency band. Let us explicitly define ω_{l_i} and ω_{h_i} as the low and high frequencies, respectively, that enclose the interval for the i-loop participation. Since $i = n$ numbers the fastest loop and $i = 1$ numbers the slowest loop, thus $\omega_{l_1} = 0$ and $\omega_{h_n} = \infty$. A sequential design of the n controllers is following proposed to carry out a quantitative allocation of the frequency band among the loops.

3.3. Robust Frequency Domain Design Method. The controllers $c_{i=1,\dots,n}$ are initially set to zero. Then, the design sequence evolves from $k = n$ to $k = 1$. When the l_k-loop design takes place at step k, c_k is the only unknown.

QFT bounds will translate the robust specifications (10) (11) in terms of the nominal open loop l_{k_o} at discrete frequencies ω. These bounds can be computed by using the command *genbnds* of Terasoft QFT Toolbox [31], which handles specifications in the general form

$$\left|\frac{A + BG}{C + DG}\right| \le W. \tag{14}$$

Therefore, specifications (10) (11) must be conveniently rewritten to identify the coefficients A, B, C, and D of (14) at each step k, being $G = c_k$. Firstly, let us group the loops already designed in the sequential procedure as

$$l_{-k} = \sum_{j=k+1}^{n} l_j, \quad k < n; \ l_{-k} \equiv \varnothing, \ k = n, \tag{15}$$

and concatenate their controllers as

$$c_{-k} = \prod_{j=k+1}^{n} c_j, \quad k < n; \ c_{-k} \equiv \varnothing, \ k = n. \tag{16}$$

Thus, (10) can be rewritten as

$$\left|\frac{p_d}{1 + l_{-k} + p_k c_{-k} c_k}\right| \le \left|W_d\right|; \quad \forall \mathbf{P}. \tag{17}$$

And the set (11) can be rewritten as two separated formulas:

$$\left|\frac{p_k c_{-k} c_k}{1 + l_{-k} + p_k c_{-k} c_k}\right| \le W_{s_k}; \quad \forall \mathbf{P}, \tag{18}$$

which cares for the stability of the k loop and the set

$$\left|\frac{l_j}{1 + l_{-k} + p_k c_{-k} c_k}\right| \le W_{s_j}, \quad j = k+1, \dots, n; \ \forall \mathbf{P}, \tag{19}$$

which cares for the stability of the loops that have already been designed. Now the control specifications (17)-(19) can be easily identified with the format (14). As an example, let us take $A = p_d$, $B = 0$, $C = 1 + l_{-k}$, $D = p_k c_{-k}$, and $W = |W_d|$ for (17).

At the k step and for a discrete frequency ω, there are a performance bound for (17) and a total amount of $n - k + 1$ stability bounds gathering (18) and (19). Let us denote $\beta_{l_k}(\omega)$ to the matching of all those bounds at certain frequency ω. A set of discrete frequencies $\omega \in [0, \infty)$ is chosen.

After computing the intersection bounds and taking into account the working frequencies for the k-loop, the nominal open-loop function $l_{k_o}(j\omega)$ is shaped fulfilling $\beta_{l_k}(\omega)$ only at $\omega_{l_k} \le \omega \le \omega_{h_k}$.

The example in Section 4.2 details thoroughly the sequential procedure for the bound computation and the loop-shaping of controllers.

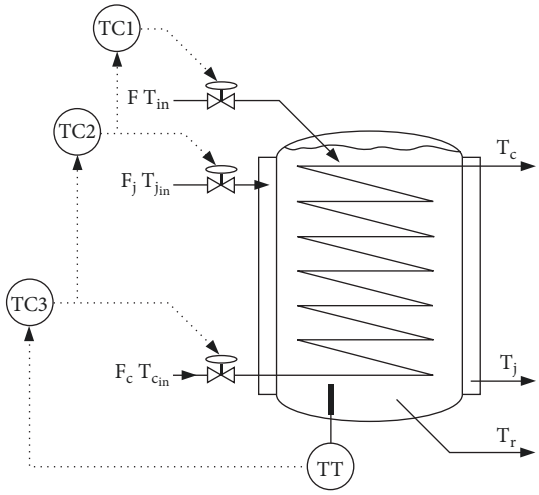

Figure 4: MISO control of cooled CSTR.

4. Example: MISO Control of Continuous Stirred-Tank Reactor

The usefulness of the proposed methodology is being illustrated through the control of a Chemical Stirred Tank Reactor (CSTR), which is a recurrent benchmark in the process control literature because of its unquestionable importance in the chemical and materials industry [21].

4.1. Continuous Stirred-Tank Reactor. A coolant flow (usually water), through either a cooling jacket or a cooling coil [32], or both [33], removes the necessary energy to prevent the exothermic and irreversible reaction runaway and to regulate the reactor temperature. Due to the limited heat-removal capacity of the coolant flow, the manipulation of the reactant flow can contribute to temperature control. Thus [21] presents a MISO strategy founded on VPC [1], which follows the classical series architecture in Figure 1. The jacket coolant flow $u_2 = F_j$ (the fastest actuation) midranges around its maximum energy removal capacity $r_{u_2} = r_{F_j}$, while large reaction temperature excursions $y = T_r$ are compensated with the feed flow-rate $u_1 = F$ (the slowest actuation). Furthermore, this smart MISO strategy achieves the highest possible production rate: F is maximised since F_j is set to maximum. Its counterpart is feed temperature $d = T_{in}$ gets a significant impact on dynamic controllability. When the feed is colder than the reactor ($T_{in} < T_r$), the immediate effect of increasing the feed flow-rate is a temporary decrease in the reactor temperature; i.e., F-T_r behaves as a nonminimum phase (NMP) plant. Then, a wise frequency distribution of MISO dynamic controllability is of importance and can be quantitatively accomplished through the robust frequency domain method that this paper develops. Beyond that and to illustrate the ability to deal with more than two manipulated inputs, the cooling capacity is being contributed from two sources: a main supply provided by a cooling jacket F_j and a quick auxiliary supply provided by a cooling coil F_c. Figure 4 shows the set-up.

Figure 5 depicts the magnitude frequency response of the linear input-output relations that intervene. In agreement

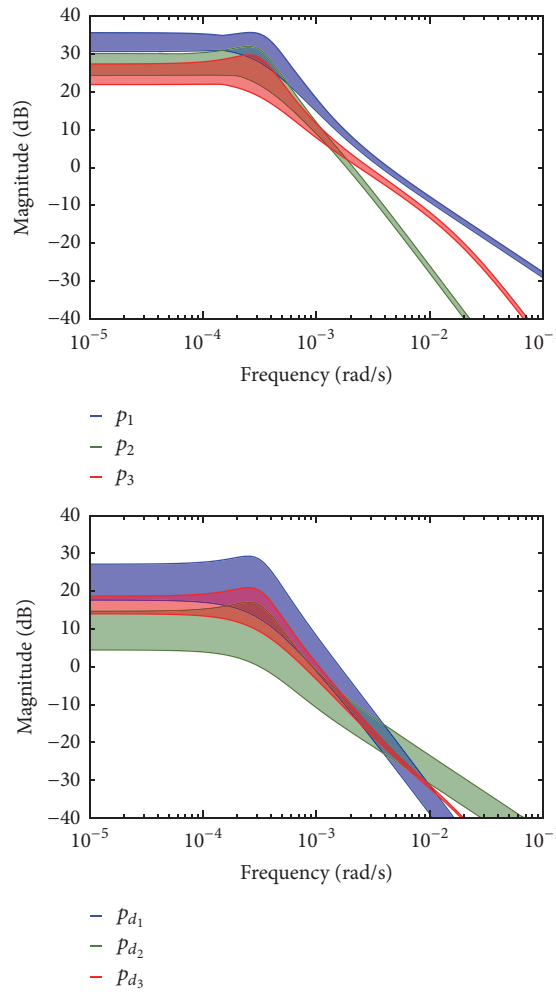

Figure 5: Plant frequency responses.

with the notation in the series control architecture (Figure 2), the contribution from the manipulated inputs, the feed flow $u_1 = F$, the jacket flow $u_2 = F_j$, and the coil flow $u_3 = F_c$, to the output, the reactor temperature $y = T_r$, yields plants p_1, p_2, and p_3, respectively. Three disturbance inputs deviate T_r: the feed concentration $d_1 = C_{a_{in}}$, the feed temperature $d_2 = T_{in}$, and the inlet coolant temperature $d_3 = T_{j_{in}} = T_{c_{in}}$, whose contributions are represented by plants p_{d_1}, p_{d_2}, and p_{d_3}, respectively. A detailed procedure on how to obtain the plant models is appended at the end of the paper. Several operating points are considered for the inputs, which yield the plant parameter uncertainty in the linearised models. A plant matrix $\mathcal{P}$ (9) collects 240 vectors $\mathbf{P} = [p_1, p_2, p_3, p_{d1}, p_{d2}, p_{d3}]$, and Figure 5 shows the envelope of their magnitude frequency responses.

It is a fact that the gain of p_1 is higher than the gain of both p_2 and p_3 along the whole frequency band. However p_1 participation will be restricted to low frequencies due to its RHP zero (increasing $u_1 = F$ produces a temporary decrease in $y = T_r$). The RHP zero that is closer to the origin for the whole p_1 uncertainty set is at $s = 9.7318 \times 10^{-4}$. Thus, $\omega = 1 \times 10^{-4}$ is chosen as the border frequency for p_1 participation. Beyond

Table 1: Frequency band allocation among $l_{i=1,2,3}$.

ω_{l_1}	$\omega_{h_1} = \omega_{l_2}$	$\omega_{h_2} = \omega_{l_3}$	ω_{h_3}
0.00	0.0001	0.001	∞

that frequency, the contribution of p_2 and p_3 will be able to improve the performance of the temperature regulation. $|p_2|$ dominates medium frequencies (ω below 1×10^{-3}) and $|p_3|$ dominates high frequencies (ω above 1×10^{-3}). This agrees with the cooling system dimensioning to the extent that the coil cooling becomes an auxiliary system with a quicker but less powerful response than the jacket cooling. Let us also mention that p_2 and p_3 have inverse gain, since raising any of the coolant flows makes the reactor temperature drop.

The other relevant point in MISO control is a convenient selection of the midrange setpoints. Since F_c is the fastest actuation, r_{F_c} is chosen at exactly the midpoint of the coolant capacity of coil cooling system to achieve maximum maneuverability. However, r_{F_j} is chosen near the maximum coolant capacity of jacket cooling system in order to F tends to maximum production rate. A reduction of r_{F_j} saves F_j but also reduces F.

4.2. MISO Robust Control of CSTR. Three performance specifications for robust disturbance rejection are defined following (10) and being p_d equal to p_{d_1}, p_{d_2}, and p_{d_3}, respectively. The required performance is that, in the case of a maximum disturbance happens, the reactor temperature deviation must be less than 0.6 K. And this maximum deviation must be reduced to 0.2 K no later than 20 min and fully extinguished in steady state. To ensure these conditions, the performance upper model is

$$\left|W_d\left(j\omega\right)\right| = \left|\frac{489.3\, j\omega}{\left(j\omega/0.003 + 1\right)^2}\right|. \tag{20}$$

The performance specification W_d has been precisely defined. It could not be achieved neither with a SISO control using the jacket flow-rate as single control variable, nor with a MISO strategy using the cooling jacket as single midrange control variable. A roughly proof of this is the cross-over frequency of the scaled plant p_2 in Figure 5. Thus the dual cooling (jacket and coil) becomes necessary, and the MISO control must have three loops (two midrange inputs).

To guarantee minimum phase margins of 30° (13) on each i-loop, three robust stability specifications (11) take as upper tolerance

$$W_{s_i} = 1.932. \tag{21}$$

The discrete set of ω-frequencies to compute QFT templates and bounds is

$$\Omega = [0.1, 1, 3, 5, 7, 10, 20, 30, 50] \times 10^{-4}. \tag{22}$$

Section 3.3 detailed the procedure for QFT bound computation that represented the robust specifications. Eventually, an intersection bound set $\beta_{l_i}(\omega)$, $\omega \in \Omega$, is obtained. Then, the shaping of $l_{i_o}(j\omega)$ is performed. In accordance to comments on plant peculiarities in Section 4.1, Table 1 shows the frequency band distribution among loops to be achieved. The sequential design of controllers c_3, c_2, and c_1 is performed as follows; Figure 6 illustrates it. Each row of plots matches a step, which is designated by the loop under design k, and each column of plots depicts bounds $\beta_{l_i}(\omega)$ and nominal open-loop function $l_{i_o}(j\omega)$ of the i-loop; different line colours distinguish the frequencies in (22).

$k = 3$ The procedure begins with the design of controller c_3 in the fastest loop l_3. As the other controllers are initially taken as zero, thus $l_1 = l_2 = 0$ and l_t reduces to solely l_3. Hence, bounds at Figures 6(a), 6(b), and 6(c) reveal a situation where l_3 should assume the whole control task and no bounds appear for $l_{i=1,2}$; see Figures 6(a) and 6(b). Bounds β_{l_3} are computed from (17) (18) with $l_{-3} \equiv c_{-3} \equiv \varnothing$. However, l_{o_3} shaping must only assume the control task over its working frequencies; i.e., l_{o_3} must only meet those β_{l_3} over $\omega \geq 0.001$. The design procedure is driven as usual in QFT: loop gain is conveniently adjusted to bounds from $\omega = 0.001$ to roll off frequencies; see Figure 6(c). It yields

$$c_3(s) = -\frac{1.6}{\left(s/0.02 + 1\right)^2}. \tag{23}$$

The negative gain of controller (23) is due to p_3 being inverse gain.

$k = 2$ It is aimed as the design of c_2 as part of the loop l_2. Now only c_1 controller is zero, and $l_t = l_3 + l_2$; i.e., both loops should contribute to the regulation task. As $l_1 = 0$, this loop does not intervene and there are no bounds for it; see Figure 6(d). Taking $l_{-2} = l_3$ and $c_{-2} = c_3$, bounds β_{l_2} are computed from (17) (18) (19); see Figure 6(e). At frequencies where l_{3_o} met its bounds, i.e., over $\omega \geq 0.001$, β_{l_2} bounds become closed forbidden regions, which prevents l_{2_o} from being in counterphase with l_{3_o}, and consequently spoiling the previously achieved performance or violating robust stability. Due to the residual gain contributed by l_{3_o} over $\omega < 0.001$, β_{l_2} bounds show dips at certain phases. Then, l_{o_2} loopshaping is performed meeting β_{l_2} over $\omega \geq 0.0001$. It yields

$$c_2(s) = \frac{5.5\left(s/0.0012 + 1\right)}{\left(s/0.00018 + 1\right)\left(s/0.01 + 1\right)^2}. \tag{24}$$

Owing to the series structure l_2 includes c_3 (6). As c_3 (23) had negative gain, c_2 (24) must have positive gain despite p_2 having inverse gain. Furthermore, c_2 adds zeros-poles at lower frequencies than c_3 did, if needed. Thus, the series arrangement lowers the order of controllers. Once c_2 is designed, the bounds β_{l_3} can be updated as Figure 6(f) depicts. Comparing it with Figure 6(c), let us note as l_{3_o} now meets bounds that were before violated (β_{l_3} over $0.0001 \leq \omega < 0.001$) since the specifications have already been achieved at these frequencies by l_2.

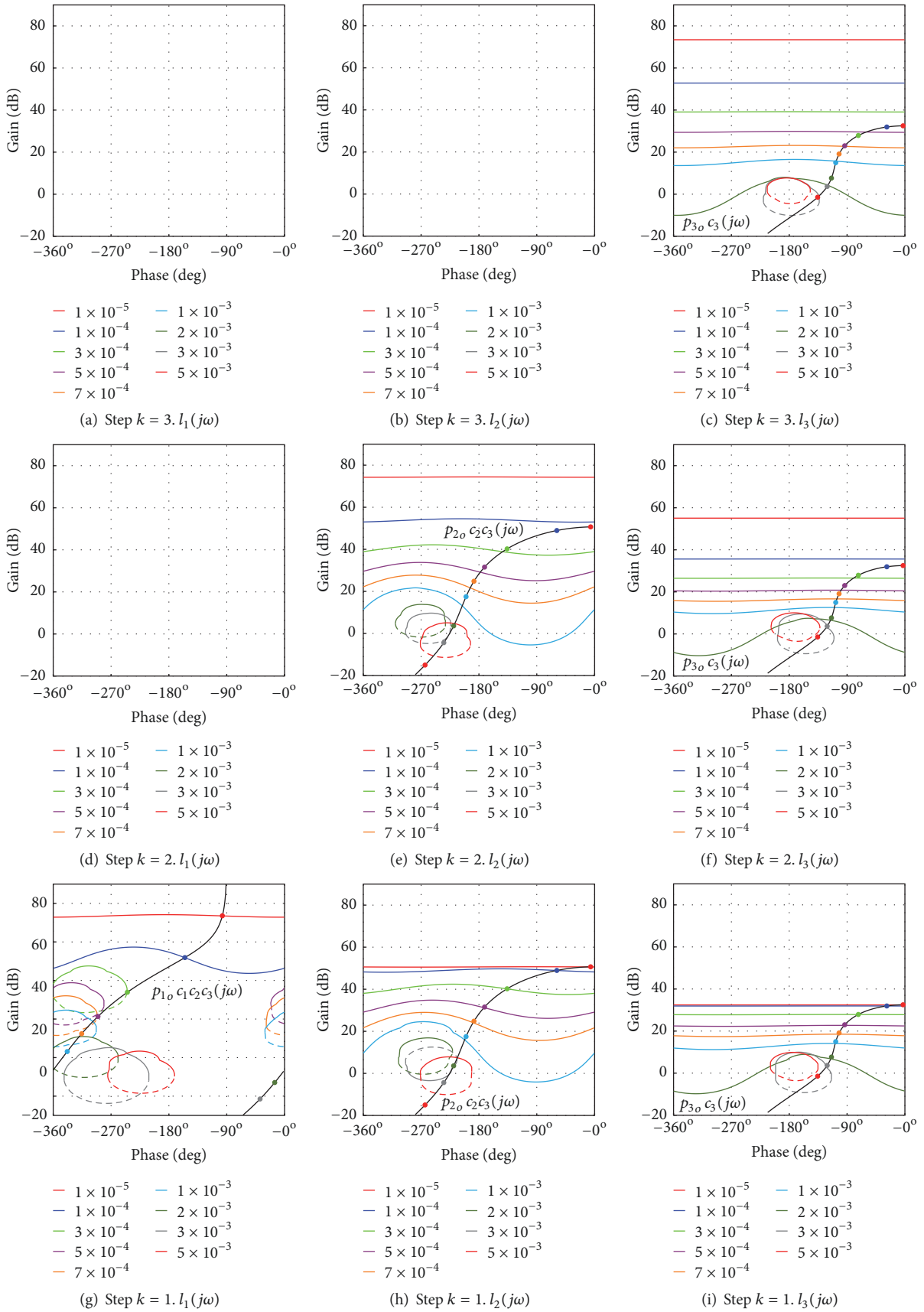

(a) Step $k = 3$. $l_1(j\omega)$ (b) Step $k = 3$. $l_2(j\omega)$ (c) Step $k = 3$. $l_3(j\omega)$

(d) Step $k = 2$. $l_1(j\omega)$ (e) Step $k = 2$. $l_2(j\omega)$ (f) Step $k = 2$. $l_3(j\omega)$

(g) Step $k = 1$. $l_1(j\omega)$ (h) Step $k = 1$. $l_2(j\omega)$ (i) Step $k = 1$. $l_3(j\omega)$

Figure 6: Bounds and loop-shaping for each loop (column) and design step (row).

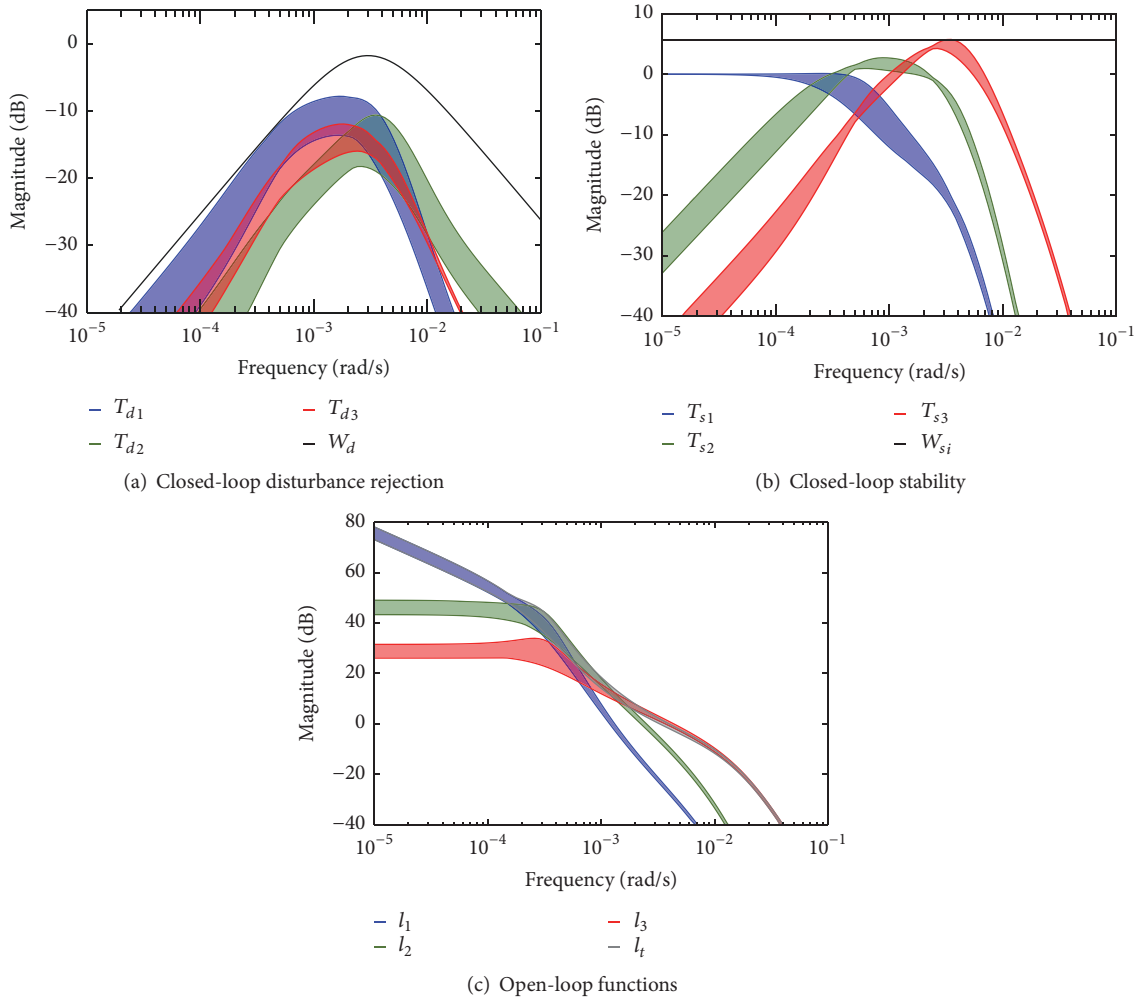

(a) Closed-loop disturbance rejection

(b) Closed-loop stability

(c) Open-loop functions

Figure 7: Frequency responses.

$k = 1$ The procedure ends with the design of c_1 in the slowest loop l_1. Taking $l_{-1} = l_3 + l_2$ and $c_{-1} = c_3 c_2$, bounds β_{l_1} are computed from (17) (18) (19); see Figure 6(g). They reveal the frequencies where l_{1_o} is required to achieve the performance; i.e., β_{l_1} bounds depict nonclosed regions over $\omega < 0.0001$. The loopshaping of l_{o_1} yields

$$c_1(s) = -\frac{0.00015}{s}. \tag{25}$$

As l_1 includes $c_2 c_3$ (6); c_1 just has to append dynamics at frequencies below those contributed by c_2 (24). One integrator in c_1 suffices for zero steady-state error at the output and at the two midrange actuations. c_1 negative gain cancels c_3 negative gain (23) in (6) since p_1 does not have inverse gain. Bounds β_{l_2} and β_{l_3} can be now updated; see Figures 6(h) and 6(i). Let us note that l_{2_o} and l_{3_o} now meet their bounds at the whole frequency band. All branches now participate in the regulation task $l_t = l_3 + l_2 + l_1$ as Table 1 required.

Figure 7 proves the fulfilment of control specifications for the whole set of 240 plant cases: (a) what concerns the robust rejection at the output of the three disturbance inputs; (b) what concerns the robust stability of the three loops; (c) what concerns the frequency band allocation among loops. Let us remark the smooth disconnection of loops around their switching frequencies, which preserves stability and avoids higher order of controllers. Beyond its switching frequency a steep gain reduction of l_i saves the amount of feedback in favour of a smaller v-sensor noise amplification at the actuator u_i (Horowitz's *cost of feedback* [26]).

Closed-loop time responses of main system variables are in Figure 8. These results have been obtained using the proposed control system in the nonlinear model of CSTR (at this point it is recommended to see the annex for a full understanding of the physical units and experiments). The simulation shows the system behaviour for step-type changes: in the feed concentration ($\delta C_{a_{in}} = +10\% C_{a_{in_o}}$ at $t = 2$ h), in the feed temperature ($\delta T_{in} = +5$ K at $t = 8$ h), and in the coolant temperature ($\delta T_{j_{in}} = -5$ K at $t = 14$ h). Several operating points have been tested, which correspond to jacket flow set-points r_{F_j} between 50% and 70% of F_j maximum cooling capacity and a coil flow set-point r_{F_c} at the midrange point (50%) of F_c maximum cooling capacity. In all cases, when

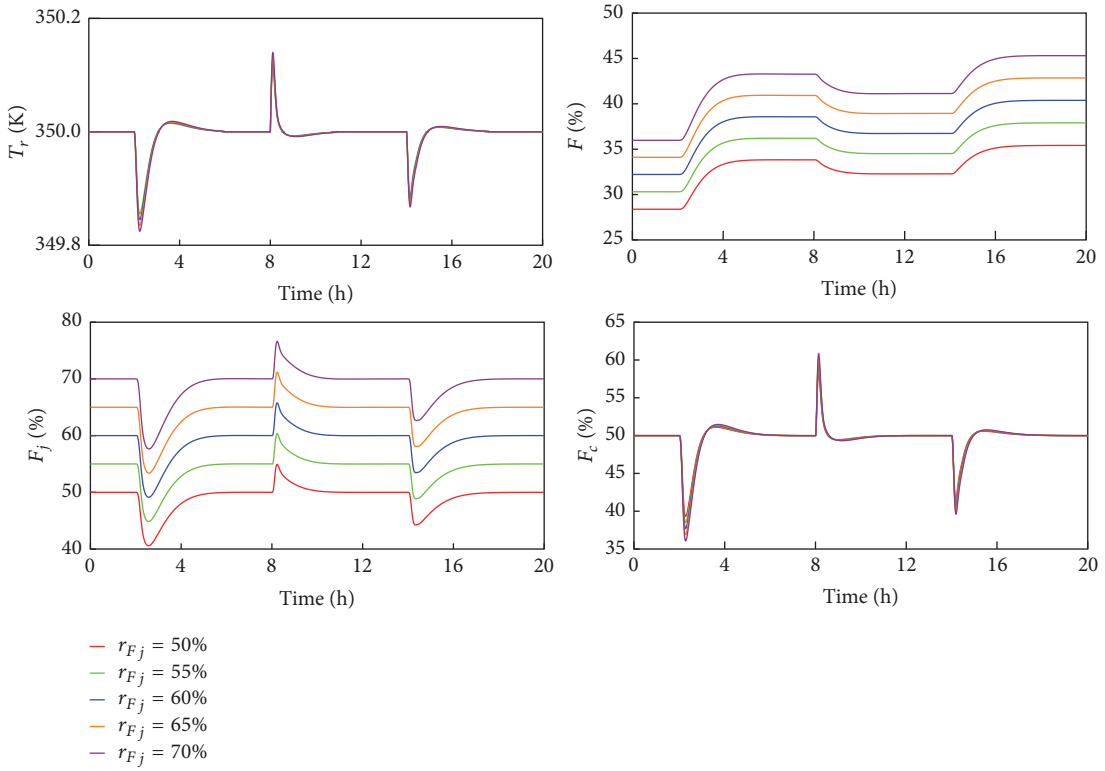

Figure 8: Closed-loop time responses.

any disturbance happens the reactor temperature T_r deviates from the set-point (r_{T_r} = 350 K) less than the maximum permitted 0.6 K and less than 0.2 K after 0.33 h. The actuator collaboration is as follows. When a disturbance happens, the coil flow F_c quickly reacts to initially compensate the reactor temperature deviation. Its intervention is progressively reset by the jacket flow F_j, when this takes control of the regulation task. As long as F_c finally returns to the midrange r_{F_c}, maximum maneuverability is preserved if another disturbance happened. Finally, F dominates the situation, and this returns F_j to r_{F_j}. Let us note that larger r_{F_j} involves larger F; i.e., it pursues increasing the production rate. On the other hand, a smaller r_{F_j} pursues saving the amount of F_j. In summary, the use of three manipulated inputs allowed not only improving the performance but also enhancing the controllability. As a matter of fact three variables are controlled, the output and two manipulated inputs.

5. Conclusions

This paper highlighted the relevance of a frequency domain method to design feedback controllers inside a new series architecture that involved several manipulated inputs. They not only intervened in the dynamic regulation of the output but also in returning all but one of the manipulated inputs to conveniently chosen set-points (midrange inputs).

Controllers and loops were arranged to participate in a series fashion when a disturbance deviated the output: the fastest open loop transfer function included a single controller, meanwhile the slowest open loop incorporated the whole set of controllers in cascade. The novelty of the new series architecture was that the controllers were on the feedback path instead of on the direct path to the midrange input set-points, as it happened in classical structures (*valve position control* or *midranging control*). In this way, integral action was only needed in the controller next to the slowest actuation to achieve zero steady state error at the regulated variables (output and midrange inputs). Since the stability of each loop was not compromised any more by a high number of integrators, the procedure to design the controllers became easier and the order of controllers was lower, especially when the number of manipulated inputs increased.

Concerning the controller design method, the frequency band was allocated among the loops that had to work together to achieve certain robust performance in disturbance rejection. Robust stability was also of concern. Achieved stability margins were linked to the uncertainty of input-output plant models. Quantitative Feedback Theory was the framework for robust control design. The multi-loop design was accomplished in a sequential way in order to use well-known tools to compute QFT bounds, which represented the robust performance and stability. A method was proposed to shape each loop according to the bounds and the frequency allocation.

As a challenging example the temperature of a chemical stirred tank reactor was regulated manipulating coil and jacket cooling flows, and the reactant flow, despite several conditions on the flow temperatures and the feed concentration tried to deviate the desired temperature in the reactor. Besides, the cooling flows were regulated to certain set-points to achieve maximum maneuverability and to manage

Table 2: Parameters and initial conditions for irreversible exothermic liquid-phase reaction A $\longrightarrow$ B; reactor parameters.

	Unit	Value
Reaction rate pre-exponential factor k_0	s^{-1}	20.75×10^6
Activation energy E	J/kmol	69.71×10^6
Process molecular weight	kg/kmol	100
Process densities ρ_{in} and ρ	kg/m^3	801
Coolant density ρ_j, ρ_c	kg/m^3	1000
Process heat capacities $c_{p_{in}}$ and c_p	$Jkg^{-1}K^{-1}$	3137
Coolant heat capacity c_{p_j}, c_{p_c}	$Jkg^{-1}K^{-1}$	4183
Heat of reaction λ	J/kmol	-69.71×10^6
Feed concentration $C_{a_{in}}$	$kmol/m^3$	8.01
Feed temperature T_{in}	K	290.00
Inlet coolant temperature $T_{j_{in}}$, $T_{c_{in}}$	K	290.00
Overall heat transfer coefficient U	$Wm^{-2}K^{-1}$	851

the production rate. The system frequency responses under different operating conditions allowed the frequency band allocation among the three loops in a quantitative way. The provided QFT control design method achieved a frequency distribution of the best MISO controllability in order to meet prescribed specifications on robust performance and stability.

Appendix

CSTR Dimensioning and Dynamic Modelling

A dual cooling CSTR (Figure 4) was used in the example of Section 4. This CSTR has been dimensioning mainly following the procedure in [21], which has been conveniently modified to split the cooling capacity into two: the jacket and coil cooling systems. An α-parameter distributes their participation: $\alpha = 1$ means a coil-full cooling and $\alpha = 0$ means a jacket-full cooling.

Process parameters and reaction initial conditions are in Table 2. In the nominal equilibrium the following is adopted: a reactor temperature of $T_{r_o} = 350$K, a conversion level of $x = 90\%$, a cooling distribution of $\alpha = 0.25$, and a feed flow-rate of $F_o = 4.377 \times 10^{-4} m^3/s$. Then, considering mass and energy equations, the cooling CSTR is sized and the nominal equilibrium is computed for the remaining variables. Table 3 collects the most relevant values. Let us remark as the nominal values for the manipulated inputs F_o, F_{j_o} and F_{c_o} mean 37%, 65%, and 50% of full capacities F_{max}, $F_{j_{max}}$, and $F_{c_{max}}$, respectively.

The system behaviour can be modelled by the following nonlinear ordinary differential equations:

(i) Component A balance:

$$\frac{dC_a(t)}{dt} = \frac{F(t)}{V_r}\left(C_{a_{in}}(t) - C_a(t)\right) - k(t)\,C_a(t) \tag{A.1}$$

(ii) Reaction rate:

$$k(t) = k_o e^{-E/RT_r(t)} \tag{A.2}$$

(iii) Reactor energy balance:

$$\begin{aligned}\frac{dT_r(t)}{dt} = {} & \frac{F(t)}{V_r}\left(T_{in}(t) - T_r(t)\right) - \frac{\lambda}{\rho c_p}k(t)\,C_a(t) \\ & - \frac{UA_j}{V_r \rho c_p}\left(T_r(t) - T_j(t)\right) \\ & - \frac{UA_c}{V_r \rho c_p}\left(T_r(t) - T_c(t)\right).\end{aligned} \tag{A.3}$$

(iv) Jacket energy balance:

$$\begin{aligned}\frac{dT_j(t)}{dt} = {} & \frac{UA_j}{V_j \rho c_{p_j}}\left(T_r(t) - T_j(t)\right) \\ & - \frac{F_j}{V_j}\left(T_j(t) - T_{j_{in}}(t)\right),\end{aligned} \tag{A.4}$$

(v) Coil energy balance:

$$\begin{aligned}\frac{dT_c(t)}{dt} = {} & \frac{UA_c}{V_c \rho c_{p_c}}\left(T_r(t) - T_c(t)\right) \\ & - \frac{F_c}{V_c}\left(T_c(t) - T_{c_{in}}(t)\right),\end{aligned} \tag{A.5}$$

Coil energy balance (A.5) is a simplification to obtain a small-signal linear model later. However, for nonlinear simulations in Figure 8, the coil is divided in $n = 40$ segments whose dynamic behaviour yields:

$$\begin{aligned}\frac{V_c \rho_c c_{p_c}}{n}\frac{dT_i(t)}{dt} = {} & \frac{UA_c}{n}\left(T_r(t) - T_i(t)\right) \\ & - F_c(t)\,\rho_c c_{p_c}\left(T_i(t) - T_{i-1}(t)\right),\end{aligned} \tag{A.6}$$

and

$$Q_i(t) = \frac{UA_c}{n}\left(T_r(t) - T_c(t)\right), \tag{A.7}$$

Table 3: Jacket-coil cooling CSTR: dimensioning and nominal case.

	Unit	Value
Nominal feed flow-rate F_o	kmol/s	4.37×10^{-4}
Nominal reactor temperature T_{r_o}	K	350.00
Conversion level x	%	90
Coolant distribution α	—	0.25
Volume of the vessel V_r	m^3	4.77
Diameter of the vessel D	m	1.45
Length of the vessel L	m	2.90
Vessel aspect ratio L/D	—	2
Jacket thickness E_j	m	2.00×10^{-1}
Jacket heat transfer area A_j	m^2	13.24
Jacket volume V_j	m^3	2.65
Coil pipe diameter d_c	m	5.08×10^{-2}
Coil loop diameter factor β	—	0.8
Number of coils N_L	—	7
Coil heat transfer area A_c	m^2	4.08
Coil volume V_c	m^3	5.15×10^{-2}
Nominal reactant concentration C_{a_o}	$kmol/m^3$	0.80
Nominal jacket flow-rate F_{j_o}	kmol/s	5.50×10^{-4}
Nominal coil flow-rate F_{c_o}	kmol/s	1.52×10^{-4}
Nominal jacket temperature T_{j_o}	K	339.80
Nominal coil temperature T_{c_o}	K	349.72
Maximum feed flow-rate F_{max}	kmol/s	11.96×10^{-4}
Maximum jacket flow-rate $F_{j_{max}}$	kmol/s	8.45×10^{-4}
Maximum coil flow-rate $F_{c_{max}}$	kmol/s	3.04×10^{-4}

where $T_{i-1}(t)$ is the temperature at the input of the i-segment, T_i the temperature at the output of the i-segment, and Q_i is the energy exchanged with the reactor along the i-segment. The total energy that is absorbed by the $i = 1, .., n$ segments of the coil is

$$Q_c(t) = \sum_{i=1}^{n} Q_i(t). \tag{A.8}$$

The nonlinear equations (A.1)-(A.5) are linearised around certain steady-state values of the system variables. It yields the small-signal linear model in (A.9), where the equilibrium of a variable is denoted by an upper bar and the small deviation of variables around equilibrium is denoted with the δ-symbol. There is supposed to be the same inlet coolant temperature at both cooling systems, i.e., $T_{j_{in}} = T_{c_{in}}$.

$$\begin{bmatrix} \delta\dot{C}_a(t) \\ \delta\dot{T}_r(t) \\ \delta\dot{T}_j(t) \\ \delta\dot{T}_c(t) \end{bmatrix} = \begin{bmatrix} -\frac{\overline{F}}{V_r} - \overline{k} & -\frac{\overline{C}_a \overline{k} E}{R\overline{T}_r^2} & 0 & 0 \\ -\frac{\lambda\overline{k}}{\rho c_p} & -\frac{\overline{F}}{V_r} - \frac{\lambda\overline{C}_a\overline{k}E}{\rho c_p R\overline{T}_r^2} - \frac{UA_j}{V_r\rho c_p} - \frac{UA_c}{V_r\rho c_p} & \frac{UA_j}{V_r\rho c_p} & \frac{UA_c}{V_r\rho c_p} \\ 0 & \frac{UA_j}{V_j\rho c_{p_j}} & -\frac{UA_j}{V_j\rho c_{p_j}} - \frac{\overline{F}_j}{V_j} & 0 \\ 0 & \frac{UA_c}{V_r\rho c_{p_c}} & 0 & -\frac{UA_c}{V_r\rho c_{p_c}} - \frac{\overline{F}_c}{V_c} \end{bmatrix} \begin{bmatrix} \delta C_a(t) \\ \delta T_r(t) \\ \delta T_j(t) \\ \delta T_c(t) \end{bmatrix}$$

$$+\begin{bmatrix} \dfrac{\overline{C}_{a_{in}}-\overline{C}_a}{V_r} & 0 & 0 & \dfrac{\overline{F}}{V_r} & 0 & 0 \\ \dfrac{\overline{T}_{in}-\overline{T}_r}{V_r} & 0 & 0 & 0 & \dfrac{\overline{F}}{V_r} & 0 \\ 0 & -\dfrac{\left(\overline{T}_j-\overline{T}_{j_{in}}\right)}{V_j} & 0 & 0 & 0 & \dfrac{\overline{F}_j}{V_j} \\ 0 & 0 & -\dfrac{\left(\overline{T}_c-\overline{T}c_{in}\right)}{V_c} & 0 & 0 & \dfrac{\overline{F}_c}{V_c} \end{bmatrix} \begin{bmatrix} \delta F(t) \\ \delta F_j(t) \\ \delta F_c(t) \\ \delta C_{a_{in}}(t) \\ \delta T_{in}(t) \\ \delta T_{j_{in}}(t) \end{bmatrix} \tag{A.9}$$

An effective control of CSTR should consider several operating points. The set of main process variables at certain equilibrium

$$\mathbf{q}_j = \left[\overline{T}_r, \overline{F}, \overline{F}_j, \overline{F}_c, \overline{C}_{a_{in}}, \overline{T}_{in}, \overline{T}_{j_{in}}\right] \tag{A.10}$$

consists of output, three manipulated inputs, and three disturbance inputs. Then, several equilibria $\mathbf{q}_j$ are being considered. Since the reactor temperature is the controlled variable, let us adopt a single equilibrium for it: $\overline{T}_r = T_{r_o}$. The three disturbance inputs are taken as independent variables, whose equilibrium values are estimated as

$$\overline{C}_{a_{in}} = \{0.9, 1.0, 1.1\} \times C_{a_{in_o}}, \tag{A.11}$$

being $C_{a_{in_o}} = 8.01$ the nominal feed concentration;

$$\overline{T}_{in} = \{285, 288, 290, 295\}, \tag{A.12}$$

which represents a variation range of ±5 around nominal $T_{in_o} = 290$, and

$$\overline{T}_{j_{in}} = \{285, 288, 290, 295\}, \tag{A.13}$$

which represents a variation range of ±5 around nominal $T_{j_{in_o}} = 290$. The cooling flow-rates must return to desired set-points after temperature regulation. Therefore, they complete the set of independent variables. The coil flow-rate is the fastest actuation for reactor temperature recovering. Thus the coil-flow set-point is fixed at the middle of its range to preserve maximum maneuverability, which means $\overline{F}_c = 0.5F_{c_{\max}}$. The jacket flow-rate set-point can be conveniently moved such that

$$\overline{F}_j = \{0.50, 0.55, 0.60, 0.65, 0.70\} \times F_{j_{max}}. \tag{A.14}$$

Let us remark that larger $\overline{F}_j$ involves larger $\overline{F}$, which increases the production rate. The combination of all possible values in (A.11), (A.12), (A.13), and (A.14) yields 240 cases. $\overline{T}_r = T_{r_o}$ and $\overline{F}_c = F_{c_o}$ complete the set of independent variables for each of the 240 operating points. Substituting them in (A.9), the dependent variable $\overline{F}$ can be computed. Eventually, (A.9) models the system dynamic behaviour for 240 operating points $\mathbf{q}_j$ (A.10).

Applying the Laplace transform to (A.9), and conveniently rearranging the equations, it yields the transfer functions:

$$m_{j=1,\ldots,6}(s) = \frac{b_{j_3}s^3 + b_{j_2}s^2 + b_{j_1}s + b_{j_0}}{s^4 + a_3s^3 + a_2s^2 + a_1s + a_0}, \tag{A.15}$$

being $m_1 = \Delta T_r/\Delta F$, $m_2 = \Delta T_r/\Delta F_j$, $m_3 = \Delta T_r/F_c$, $m_4 = \Delta T_r/\Delta C_{a_{in}}$, $m_5 = \Delta T_r/\Delta T_{in}$, and $m_6 = \Delta T_r/\Delta T_{j_{in}}$. Coefficients b_{j_k} and a_k $(j = 1, \ldots, 6;\ k = 0, \ldots, 3)$ depend on process parameters (see Tables 2 and 3) and on the 240 equilibrium values $\mathbf{q}_j$.

Multivariable systems must be conveniently scaled for control design tasks [19]. Here the presence of a single output makes only necessary to scale the ranges of the five inputs. The scaling gains for $C_{a_{in}}$, T_{in}, and $T_{j_{in}}$ are $0.1C_{a_{in_o}}$, 5, and 5, respectively, according to the smallest distance from $C_{a_{in_o}}$, T_{in_o}, and $T_{j_{in_o}}$ to the edge of intervals (A.11), (A.12), and (A.13), respectively. The scaling gain for F_j is $0.3F_{j_{\max}}$ according to the smallest distance from any equilibrium value $\overline{F}_j$ (A.14) to the maximum capacity $F_{j_{\max}}$. In a similar way a scaling gain of $0.254F_{\max}$ for F and a scaling gain of $0.5F_{c_{\max}}$ for F_c is computed. These scaling gains are applied to plants (A.15). Eventually, the plant matrix $\mathscr{P}$ is obtained which collects 240 vectors $\mathbf{P}(s; q_j) = [p_1, p_2, p_3, p_{d_1}, p_{d_2}\ p_{d_3}]$, whose magnitude frequency response is depicted in Figure 5.

Data Availability

The data used to support the findings of this study are available from the corresponding author upon request.

Conflicts of Interest

The authors declare that they have no conflicts of interest.

Acknowledgments

The authors are grateful for the assistance provided by University of La Rioja.

References

[1] F. G. Shinskey, "Control systems can save energy," *Chemical Engineering Progress*, vol. 740, no. 5, pp. 43–46, 1978.

[2] O. Prado-Rubio, S. Jørgensen, and G. Jonsson, "pH control structure design for a periodically operated membrane separation process," *Computers & Chemical Engineering*, vol. 43, pp. 120–129, 2012.

[3] O. Johnsson, D. Sahlin, J. Linde, G. Lidén, and T. Hägglund, "A mid-ranging control strategy for non-stationary processes and its application to dissolved oxygen control in a bioprocess," *Control Engineering Practice*, vol. 42, pp. 89–94, 2015.

[4] S. Nájera, M. Gil-Martínez, and J. Rico-Azagra, "Dual-control of autothermal thermophilic aerobic digestion using aeration and solid retention time," *Water (Switzerland)*, vol. 9, no. 6, 2017.

[5] S. Haugwitz, P. Hagander, and T. Norén, "Modeling and control of a novel heat exchange reactor, the open plate reactor," *Control Engineering Practice*, vol. 150, no. 7, pp. 779–792, 2007.

[6] M. Karlsson, O. Slätteke, B. Wittenmark, and S. Stenström, "Reducing moisture transients in the paper-machine drying section with the mid-ranging control technique," *Nordic Pulp & Paper Research Journal* , vol. 20, no. 2, pp. 150–155, 2005.

[7] J. Sun, F. Cameron, and B. W. Bequette, "A habituating blood glucose control strategy for the critically ill," *Journal of Process Control*, vol. 22, no. 8, pp. 1411–1421, 2012.

[8] K. Van Heusden, J. M. Ansermino, and G. A. Dumont, "Robust MISO Control of Propofol-Remifentanil Anesthesia Guided by the NeuroSENSE Monitor," *IEEE Transactions on Control Systems Technology*, 2017.

[9] N. Ravi, H.-H. Liao, A. F. Jungkunz, H. H. Song, and J. C. Gerdes, "Modeling and control of exhaust recompression HCCI: Split fuel injection for cylinder-individual combustion control," *IEEE Control Systems Magazine*, vol. 32, no. 4, pp. 26–42, 2012.

[10] S. Jade, E. Hellström, J. Larimore, A. G. Stefanopoulou, and L. Jiang, "Reference governor for load control in a multicylinder recompression HCCI engine," *IEEE Transactions on Control Systems Technology*, vol. 22, no. 4, pp. 1408–1421, 2014.

[11] S. J. Schroeck, W. C. Messner, and R. J. McNab, "On compensator design for linear time-invariant dual-input single-output systems," *IEEE/ASME Transactions on Mechatronics*, vol. 6, no. 1, pp. 50–57, 2001.

[12] M. Kobayashi and R. Horowitz, "Track seek control for hard disk dual-stage servo systems," *IEEE Transactions on Magnetics*, vol. 37, no. 2 I, pp. 949–954, 2001.

[13] U. Schneider, B. Olofsson, O. Sörnmo et al., "Integrated approach to robotic machining with macro/micro-actuation," *Robotics and Computer-Integrated Manufacturing*, vol. 30, no. 6, pp. 636–647, 2014.

[14] T. Haus, A. Ivanovic, M. Car, M. Orsag, and S. Bogdan, "Mid-Ranging Control Concept for a Multirotor UAV with Moving Masses," in *Proceedings of the 26th Mediterranean Conference on Control and Automation (MED '18)*, pp. 339–344, Zadar, June 2018.

[15] M. A. Henson, B. A. Ogunnaike, and J. S. Schwaber, "Habituating control strategies for process control," *AIChE Journal*, vol. 41, no. 3, pp. 604–618, 1995.

[16] Javier Rico-Azagra, Montserrat Gil-Martínez, and Jorge Elso, "Quantitative Feedback Control of Multiple Input Single Output Systems," *Mathematical Problems in Engineering*, vol. 2014, Article ID 136497, 17 pages, 2014.

[17] B. J. Allison and A. J. Isaksson, "Design and performance of mid-ranging controllers," *Journal of Process Control*, vol. 8, no. 5-6, pp. 469–474, 1998.

[18] W. L. Luyben, *Process Modelling, Simulation and Control for Chemical Engineers*, McGraw-Hill Education, 1989.

[19] S. Skogestad and I. Postlethwaite, *Multivariable feedback control. Analysis and design*, John Wiley & Sons Ltd, 2005.

[20] K. Aström and T. Hägglund, "Advanced PID control," *ISA-The Instrumentation, Systems and Automation Society*, 2009.

[21] W. L. Luyben, *Chemical Reactor Design and Control*, John Wiley & Sons, Inc., Hoboken, NJ, USA, 2007.

[22] C.-C. Yu and W. L. Luyben, "Analysis of Valve-Position Control for Dual-Input Processes," *Industrial & Engineering Chemistry Fundamentals*, vol. 25, no. 3, pp. 344–350, 1986.

[23] B. J. Allison and S. Ogawa, "Design and tuning of valve position controllers with industrial applications," *Transactions of the Institute of Measurement and Control*, vol. 25, no. 1, pp. 3–16, 2003.

[24] J. Alvarez-Ramirez, A. Velasco, and G. Fernandez-Anaya, "A note on the stability of habituating process control," *Journal of Process Control*, vol. 14, no. 8, pp. 939–945, 2004.

[25] B. Sun, S. Skogestad, J. Lu, and W. Zhang, "Dual SIMC-PI Controller Design for Cascade Implement of Input Resetting Control with Application," *Industrial & Engineering Chemistry Research*, vol. 57, no. 20, pp. 6947–6955, 2018.

[26] I. Horowitz, "Survey of quantitative feedback theory (QFT)," *International Journal of Robust and Nonlinear Control*, vol. 11, no. 10, pp. 887–921, 2001.

[27] M. Sidi, *Desing of robust control systemns from clasical to modern practical approaches*, Kreieger publishing company, 2001.

[28] M. Garcia-Sanz, *Robust Control Engineering: Practical QFT Solutions*, CRC Press, 2017.

[29] J. Rico-Azagra, M. Gil-Martínez, R. Rico, and P. Maisterra, "Qft bounds for robust stability specifications defined on the open-loop function," *International Journal of Robust and Nonlinear Control*, vol. 280, no. 3, pp. 1116–1125, 2018.

[30] I. Horowitz, *Quantitative Feedback Design Theory (QFT)*, QFT Publications, 1993.

[31] C. Borghesani, Y. Chait, and O. Yaniv, *Quantitative Feedback Theory Toolbox. For use with Matlab*, Terasoft, 2nd edition, 2002.

[32] W. L. Luyben, "Quantitative comparison of temperature control of reactors with jacket cooling or internal cooling coils," *Industrial & Engineering Chemistry Research*, vol. 43, no. 11, pp. 2691–2703, 2004.

[33] Z. Wang and Q. Peng, "Temperature fault-tolerant control system of the CSTR with coil and jacket cooling based on VPC," in *In Proceedings of the 27th Control and Decision Conference (CCDC '15)*, pp. 3885–3890, 2015.